New Journal of Physics
An Institute of Physics and Deutsche Physikalische Gesellschaft Journal

On the measurement of two-photon single-mode coupling efficiency in parametric down-conversion photon sources

S Castelletto[1], I P Degiovanni[1], A Migdall[2] and M Ware[2]

[1] Istituto Elettrotecnico Nazionale G Ferraris, Strada delle Cacce 91-10135, Torino, Italy

[2] Optical Technology Division, National Institute of Standards and Technology, Gaithersburg, MD 20899-8441, USA

E-mail: castelle@ien.it and amigdall@nist.gov

New Journal of Physics **6** (2004) 87
Received 5 February 2004
Published 29 July 2004
Online at http://www.njp.org/
doi:10.1088/1367-2630/6/1/087

Abstract. Photon-based quantum information schemes have increased the need for light sources that produce individual photons, with many such schemes relying on optical parametric down-conversion (PDC). Practical realizations of this technology require that the PDC light be collected into a single spatial mode defined by an optical fibre. In this paper, we present two possible models to describe single-mode fibres coupling with PDC light fields in a non-collinear configuration, leading to two different results. These approaches include factors such as crystal length and walk-off, non-collinear phase-matching and also transverse pump field distribution. We propose an experimental test to distinguish between the two models. The goal is to help clarify open issues, such as how to extend the theory beyond the simplest experimental arrangements and, more importantly, to suggest ways to improve the collection efficiency.

PII: S1367-2630(04)75829-2

Contents

1. Introduction

The advent of photon-based quantum cryptography, communication and computation schemes [1]–[10] has increased the need for light sources that produce individual photons [11]. An ideal single-photon source would produce completely characterized single photons on demand. Since all the currently available sources fall significantly short of this ideal (i.e. they do not produce photons 100% of the time and/or they do not produce only single photons), much effort has been focused on creating improved approximations of single-photon-on-demand sources (SPOD) [12]–[19]. Some of these schemes [17, 19] rely on optical parametric down-conversion (PDC), because it produces photons two at a time, allowing one photon to herald the existence of the other. In a previous work, we proposed one such scheme where a multiplexed PDC array is used to make an improved SPOD source having increased probability of single-photon emission, while suppressing the probability of multi-photon generation [19]. Most PDC-based schemes (including ours) require that the PDC output be collected into a single spatial mode defined by an optical fibre. For these PDC schemes to reliably produce single photons, it is essential that the optical collection system efficiently gathers and detects the herald photon and, with minimal loss, sends its partner to the output of the system. In addition to SPOD applications, it is also important to understand collection efficiency for other applications such as PDC-based metrological applications, which are very sensitive to collection efficiency [20].

Various theoretical models have been developed to predict how the collection efficiency of PDC light in a 'two-photon single mode' can be improved [21]–[24] and, in some cases, these models have been used to improve coupling efficiency. In particular, it has been shown that the size of the pump beam focus affects the shape of the PDC output [21] and, hence, the coupling efficiency of the PDC light with a given spatial mode. In addition, a more detailed work [23] recently showed how increasing the crystal length and walk-off decreases the coupling efficiency for a pulsed broadband pump. However, in these works, attempts to increase the single-mode fibre coupling efficiency were limited to a tightly focused pump beam and a thin crystal, which reduces the overall source brightness. This last restriction is forced on the calculations because the approximations used for the phase-mismatch function in terms of longitudinal wavevector

mismatch are not valid in the long-crystal case. Moreover, these works deal only with either type I or II phase-matching conditions; they do not include the non-collinearity and/or walk-off of the emitted photons and the pump beam. The work done to date does, however, give some partial guidance for increasing the coupling efficiency in certain experimental situations. For instance, the most practical results to date generally show that the collection efficiency for long crystals is optimized for properly matched large pump and collection waists. However, the maximum efficiency is limited by walk-off in type II phase-matching [23] and by excessive crystal length in type I phase-matching [24]. Furthermore, the approximations done in the previous theory limited the validity of the results to a narrow range of crystal lengths and collection/pump waists.

A more general approach to the problem is needed to clarify open issues such as those mentioned above (i.e. overcoming the calculation limits and extending the theory) and to determine how we can best test the collection efficiency model. Here, we present a model to describe the coupling of the PDC source with single spatial modes. This method uses a field-based model to describe the coupling of the PDC field with the single-mode fibre-defined fields, as has been partially presented in other works along with some suggestive supporting data [23, 24]. We also present an alternative intensity-based model, where an intensity projector operator represents the effect of a spatial filtering, as suggested in [21, 25]. We calculate the collection efficiencies using both the methods for both type I and II PDC output into two single modes defined by optical fibres, accounting for effects due to the crystal length, walk-off of extraordinary fields, non-collinear phase-matching and pump transverse-field distribution. We then analytically evaluate both efficiencies, assuming negligible second-order terms in the transverse component of the wavevectors. The intensity-based approach exhibits counter-intuitive results, even in the thin crystal limit, and may be more suitable for multi-mode collection. We propose an experimental test to distinguish between the two.

The work is organized as follows: in section 2, we define the field- and intensity-based collection efficiencies for a PDC field. In sections 3 and 4, we explicitly calculate the two efficiencies in terms of the parameters of the physical systems. In section 5, we compare the predictions of the two models. The appendix contains the geometrical analysis of the wavevector displacement, resulting from walk-off and non-collinear phase-matching.

2. Definition of PDC field- and intensity-based collection efficiencies

To determine the collection efficiency of the parametric down-conversion output into two single spatial modes (defined in our set-up by single-mode optical fibres and lenses as shown in figure 1), we use two very different approaches. In the first, we calculate the overlap of the PDC field with the field modes selected by the fibres and indirectly evaluate coincidences and singles. In the second approach, we calculate the PDC wave function over the spatial distribution of intensities as defined by single-mode fibres, directly providing coincidences and associated single counts. The main difference between the two approaches relates to the fibre mode selection and the associated detection process. The first assumes that the fibre plus the detector is a system capable of distinguishing single-mode fields, and the calculation is therefore performed in terms of fields rather than intensities. The second approach assumes that the fibres select the mode and the detectors measure the associated intensity.

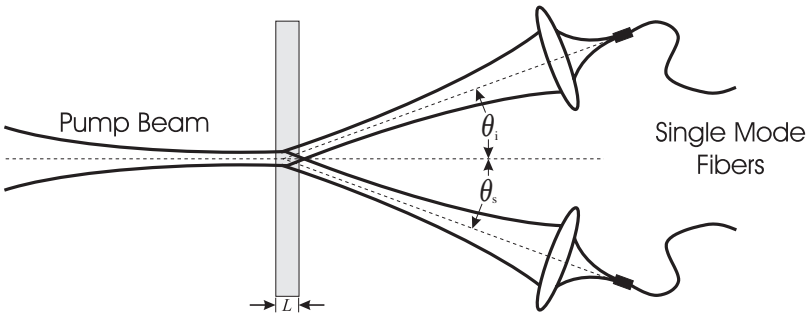

Figure 1. PDC is generated in non-linear crystals of length L by a pump beam with a Gaussian profile and collected into single-mode optical fibres as imaged by lenses.

2.1. PDC single-mode field-based collection efficiency

In the field-based approach, the first step is to calculate the two-photon PDC field [26] given by

$$A_{12}(\boldsymbol{r}_1, \boldsymbol{r}_2, t_1, t_2) = \langle 0|\widehat{E}_{\mathrm{s}}^{(+)}(\boldsymbol{r}_1, t_1)\widehat{E}_{\mathrm{i}}^{(+)}(\boldsymbol{r}_2, t_2)|\psi\rangle, \tag{1}$$

where the subscripts s, i and (later) p indicate the signal, idler and pump, respectively, and where $|0\rangle$ is the vacuum state and $|\psi\rangle$ is the two-photon wavefunction, written as

$$|\psi\rangle = \int \mathrm{d}^3 r_1\, \mathrm{d}^3 r_2\, \mathrm{d}t_1\, \mathrm{d}t_2\, \widetilde{\Phi}(\boldsymbol{r}_1, \boldsymbol{r}_2, t_1, t_2)|1_{\boldsymbol{r}_2,t_2}\rangle|1_{\boldsymbol{r}_1,t_1}\rangle, \tag{2}$$

where $\boldsymbol{r}_{1,2}$ describes the positions of the two photons at time $t_{1,2}$, and $\widetilde{\Phi}(\boldsymbol{r}_1, \boldsymbol{r}_2, t_1, t_2)$ is the phase-matching function. The fields

$$\widehat{E}_{\mathrm{s,i}}^{(+)}(\boldsymbol{r}_{1,2}, t_{1,2}) = N_{\boldsymbol{E}} \int \mathrm{d}^3 k_{\mathrm{s,i}}\, \mathrm{d}\omega_{\mathrm{s,i}}\, \hat{a}_{\boldsymbol{k}_{\mathrm{s,i}},\omega_{\mathrm{s,i}}} \exp[\mathrm{i}(\boldsymbol{k}_{\mathrm{s,i}} \cdot \boldsymbol{r}_{1,2} - \omega_{\mathrm{s,i}} t_{1,2})] \tag{3}$$

are the positive-frequency portions of the electric field operator evaluated at positions $\boldsymbol{r}_j$ and times t_j. $N_{\boldsymbol{E}}$ is a normalization factor and $\hat{a}_{\boldsymbol{k}_{\mathrm{s,i}},\omega_{\mathrm{s,i}}}$ is the photon annihilation operator. To determine the collection efficiency, we write A_{12} as a coherent superposition of guided modes $\varphi_{lm}^*(x, y)$ in the fibre, as suggested in [23]:

$$A_{12}(\boldsymbol{r}_1, \boldsymbol{r}_2, t_1, t_2) = \sum_{l'm', lm} A_{12}{}^{l'm', lm}(z_1, z_2, t_1, t_2)\varphi_{l'm'}^*(x_1, y_1)\varphi_{lm}^*(x_2, y_2). \tag{4}$$

The field-based collection efficiency can then be written as

$$\chi_{12} = \frac{\mathcal{C}_{12}}{\sqrt{\mathcal{C}_1 \mathcal{C}_2}}, \tag{5}$$

where $\mathcal{C}_{12}$ is the fractional power [27] of the biphoton field coupled with the two single-mode fibres, i.e. the overlap between the PDC field and both collection modes. Similarly, $\mathcal{C}_1$ and $\mathcal{C}_2$ are

the fractional powers of the biphoton field coupled with each single-mode fibre, defined by the overlap between the biphoton field and each collection mode:

$$\begin{aligned}
\mathcal{C}_{12} &= \int \mathrm{d}z_1\,\mathrm{d}t_1\,\mathrm{d}z_2\,\mathrm{d}t_2 \\
&\quad\times \left| \int \mathrm{d}x_1\,\mathrm{d}y_1\,\mathrm{d}x_2\,\mathrm{d}y_2\, A_{12}(\boldsymbol{r}_1, t_1, \boldsymbol{r}_2, t_2)\varphi^*_{l'm'}(x_1, y_1)\varphi^*_{lm}(x_2, y_2)\right|^2, \\
\mathcal{C}_1 &= \int \mathrm{d}z_1\,\mathrm{d}t_1\,\mathrm{d}t_2\,\mathrm{d}^3r_2 \left| \int \mathrm{d}x_1\,\mathrm{d}y_1\, A_{12}(\boldsymbol{r}_1, t_1, \boldsymbol{r}_2, t_2)\varphi^*_{l'm'}(x_1, y_1)\right|^2, \\
\mathcal{C}_2 &= \int \mathrm{d}z_2\,\mathrm{d}t_2\,\mathrm{d}t_1\,\mathrm{d}^3r_1 \left| \int \mathrm{d}x_2\,\mathrm{d}y_2\, A_{12}(\boldsymbol{r}_1, t_1, \boldsymbol{r}_2, t_2)\varphi^*_{l'm'}(x_2, y_2)\right|^2.
\end{aligned} \tag{6}$$

This approach for obtaining the efficiency χ_{12} is similar to classical photonics theory. However, the same result can obtained by a quantum mechanical approach with projectors given by

$$\widehat{P}^{(j)}_{l,m} = |1^{(j)}_{lm}\rangle\langle 1^{(j)}_{lm}|, \tag{7}$$

where

$$|1^{(j)}_{lm}\rangle = \int \mathrm{d}^2\boldsymbol{\rho}_j\, \varphi_{lm}(\boldsymbol{\rho}_j)|1_{\boldsymbol{\rho}_j}\rangle \tag{8}$$

with $j = 1, 2$. The coincidences can then be calculated by projecting the wavefunction over two single-mode fibres:

$$\mathcal{C}_{12} \propto \mathrm{Tr}[|\psi\rangle\langle\psi|\widehat{P}^{(1)}_{lm}\widehat{P}^{(2)}_{l'm'}] \tag{9}$$

and the singles are given by

$$\mathcal{C}_j \propto \mathrm{Tr}[|\psi\rangle\langle\psi|\widehat{P}^{(j)}_{lm}]. \tag{10}$$

2.2. PDC single-mode intensity-based collection efficiency

In the intensity-based approach the projectors representing the spatial distribution of a single-mode fibre are given by

$$\widehat{P}_j = \int \mathrm{d}^3r_j\,\mathrm{d}t_j\,\mathcal{I}_j(\boldsymbol{r}_j, t_j)|1_{\boldsymbol{r}_j,t_j}\rangle\langle 1_{\boldsymbol{r}_j,t_j}|, \tag{11}$$

with $j = 1, 2$. $\mathcal{I}_j(\boldsymbol{r}_j, t_j)$ are the intensity profiles of the single-mode spatial distribution of the fields. This approach is similar to the approach in [25], which considers conditionally prepared photon states. Then, the coincidences calculated by projecting the wavefunction over two single-mode fibres are

$$C_{12} = \mathrm{Tr}[|\psi\rangle\langle\psi|\widehat{P}_1\widehat{P}_2] = \int \mathrm{d}^3r_1\,\mathrm{d}^3r_2\,\mathrm{d}t_1\,\mathrm{d}t_2\,|\widetilde{\Phi}(\boldsymbol{r}_1, \boldsymbol{r}_2, t_1, t_2)|^2\mathcal{I}_1(\boldsymbol{r}_1, t_1)\mathcal{I}_2(\boldsymbol{r}_2, t_2), \tag{12}$$

and the singles are given by

$$S_j = \mathrm{Tr}[|\psi\rangle\langle\psi|\widehat{P}_j] = \int \mathrm{d}^3 r_1\, \mathrm{d}^3 r_2\, \mathrm{d}t_1\, \mathrm{d}t_2\, |\widetilde{\Phi}(\boldsymbol{r}_1, \boldsymbol{r}_2, t_1, t_2)|^2 \mathcal{I}_j(\boldsymbol{r}_j, t_j). \tag{13}$$

The single-mode intensity-based collection efficiency is then defined by

$$\eta_{12} = \frac{C_{12}}{\sqrt{S_1 S_2}}. \tag{14}$$

3. Calculation of the field-based collection efficiency

The two-photon state at the output surface of a PDC crystal, oriented with its face perpendicular to the z-axis, is given by [26]

$$|\psi\rangle = \int \mathrm{d}^3 k_\mathrm{s}\, \mathrm{d}\omega_\mathrm{s}\, \mathrm{d}^3 k_\mathrm{i}\, \mathrm{d}\omega_\mathrm{i}\, \Phi(\boldsymbol{k}_\mathrm{s}, \boldsymbol{k}_\mathrm{i}, \omega_\mathrm{i}, \omega_\mathrm{s})|1_{\boldsymbol{k}_\mathrm{s},\omega_\mathrm{s}}\rangle|1_{\boldsymbol{k}_\mathrm{i},\omega_\mathrm{i}}\rangle, \tag{15}$$

where $\Phi(\boldsymbol{k}_\mathrm{s}, \boldsymbol{k}_\mathrm{i}, \omega_\mathrm{i}, \omega_\mathrm{s})$ is given by

$$\begin{aligned}\Phi(\boldsymbol{k}_\mathrm{s}, \boldsymbol{k}_\mathrm{i}, \omega_\mathrm{i}, \omega_\mathrm{s}) = N \int \mathrm{d}^3 k_\mathrm{p}\, \mathrm{d}\omega_\mathrm{p} \int_S \mathrm{d}x\, \mathrm{d}y \int_{-L}^{0} \mathrm{d}z\, \widetilde{E}_\mathrm{p}(\boldsymbol{q}_\mathrm{p}) \mathrm{e}^{\mathrm{i}(\Delta k_x x + \Delta k_y y + \Delta k_z z)} \\ \times \delta(\omega_\mathrm{s} + \omega_\mathrm{i} - \omega_\mathrm{p})\delta(\omega_\mathrm{p} - \Omega_\mathrm{p}) \\ \times \delta\left[\boldsymbol{k}_\mathrm{p} \cdot \boldsymbol{p}_z - \sqrt{\left(\frac{n(\Omega_\mathrm{p})\Omega_\mathrm{p}}{c}\right)^2 - \boldsymbol{q}_\mathrm{p}^2}\right] \\ \times \delta\left[\boldsymbol{k}_\mathrm{s} \cdot \boldsymbol{s}_z - \sqrt{\left(\frac{n(\omega_\mathrm{s})\omega_\mathrm{s}}{c}\right)^2 - \boldsymbol{q}_\mathrm{s}^2}\right] \\ \times \delta\left[\boldsymbol{k}_\mathrm{i} \cdot \boldsymbol{i}_z - \sqrt{\left(\frac{n(\omega_\mathrm{i})\omega_\mathrm{i}}{c}\right)^2 - \boldsymbol{q}_\mathrm{i}^2}\right],\end{aligned} \tag{16}$$

where S is the cross-sectional area of the crystal illuminated by the pump, N the normalization factor and L the length of the crystal. We denote the crystal axes in the lab frame by $\boldsymbol{c}_x$, $\boldsymbol{c}_y$ and $\boldsymbol{c}_z$, with the pump beam propagating along $\boldsymbol{c}_z$. Because the signal and idler wavevectors do not generally point along the crystal axes and also because of beam walk-off, we identify the directions of the pump, signal and idler Poynting vectors as $\boldsymbol{p}_z$, $\boldsymbol{s}_z$ and $\boldsymbol{i}_z$ and their transverse components as $\boldsymbol{p}_{x,y}$, $\boldsymbol{s}_{x,y}$ and $\boldsymbol{i}_{x,y}$. Using the above notation, we evaluate $\Delta k_{x,y,z}$. Given that $\Delta k_{x,y,z} = (\boldsymbol{k}_\mathrm{p} - \boldsymbol{k}_\mathrm{s} - \boldsymbol{k}_\mathrm{i}) \cdot \boldsymbol{c}_{x,y,z}$, we write $\Delta k_{x,y,z}$ in terms of the pump, signal and idler Poynting

vectors. The longitudinal component of the pump Poynting vector is

$$\boldsymbol{k}_{\mathrm{p}} \cdot \boldsymbol{p}_z = \sqrt{\left(\frac{n(\Omega_{\mathrm{p}})\Omega_{\mathrm{p}}}{c}\right)^2 - \boldsymbol{q}_{\mathrm{p}}^2}, \tag{17}$$

where $\boldsymbol{q}_{\mathrm{p}}$ is the transverse component of the pump $\boldsymbol{k}$-vector and c is the speed of light. Analogous expressions give the signal and idler longitudinal components.

We now make some approximations to evaluate $\Delta k_{x,y,z}$. First, we assume that the pump, signal and idler have narrow transverse angular distributions, so that we can adopt the paraxial approximation. We also rewrite the longitudinal $\boldsymbol{k}$-vector components by expanding the index of refraction $n_{\mathrm{p,s,i}}(\omega_{\mathrm{p,s,i}}, \phi)$ around the central frequencies $(\Omega_{\mathrm{s,i}})$, and around the phase-matching angle ϕ_o. This last approximation holds only in cases where the considered field is an extraordinary wave (this, of course, depends on the type of phase-matching adopted, namely type I or II). In all cases, we limit our calculation to the first perturbative order. We also assume small non-collinearity and small walk-off angles. When these two approximations hold, we can expand the sine and cosine terms, limited to first order. Finally, we write the overall $\Delta k_{x,y,z}$ terms as (see the appendix for the explicit calculation)

$$\begin{aligned}
\Delta k_x &= \boldsymbol{q}_{\mathrm{p}} \cdot \boldsymbol{p}_{\boldsymbol{x}} - \boldsymbol{q}_{\mathrm{s}} \cdot \boldsymbol{s}_{\boldsymbol{x}} - \boldsymbol{q}_{\mathrm{i}} \cdot \boldsymbol{i}_{\boldsymbol{x}} - \gamma_{\mathrm{s}} K_{\mathrm{s}}, \\
\Delta k_y &= \boldsymbol{q}_{\mathrm{p}} \cdot \boldsymbol{p}_{\boldsymbol{y}} - \boldsymbol{q}_{\mathrm{s}} \cdot \boldsymbol{s}_{\boldsymbol{y}} - \boldsymbol{q}_{\mathrm{i}} \cdot \boldsymbol{i}_{\boldsymbol{y}} - \theta_{\mathrm{i}} K_{\mathrm{i}} - \theta_{\mathrm{s}} K_{\mathrm{s}}, \\
\Delta k_z &= D\nu - \gamma_{\mathrm{p}}(\boldsymbol{q}_{\mathrm{p}} \cdot \boldsymbol{p}_{\boldsymbol{x}} - \boldsymbol{q}_{\mathrm{s}} \cdot \boldsymbol{s}_{\boldsymbol{x}} - \boldsymbol{q}_{\mathrm{i}} \cdot \boldsymbol{i}_{\boldsymbol{x}}) - \gamma_{\mathrm{s}} \boldsymbol{q}_{\mathrm{s}} \cdot \boldsymbol{s}_{\boldsymbol{x}} \\
&\quad + (\mathcal{N}_{\mathrm{p}} - \mathcal{N}_{\mathrm{s}}) \frac{\boldsymbol{q}_{\mathrm{p}} \cdot \boldsymbol{p}_{\boldsymbol{y}}}{K_{\mathrm{p}}} + \theta_{\mathrm{s}} \boldsymbol{q}_{\mathrm{s}} \cdot \boldsymbol{s}_{\boldsymbol{y}} - \theta_{\mathrm{i}} \boldsymbol{q}_{\mathrm{i}} \cdot \boldsymbol{i}_{\boldsymbol{y}},
\end{aligned} \tag{18}$$

where $\theta_{\mathrm{i,s}}$ are the emission angles of the idler and signal photons, $K_{\mathrm{i,s,p}} = n_{\mathrm{i,s,p}}(\Omega_{\mathrm{i,s,p}}, \phi)\Omega_{\mathrm{i,s,p}}/c$ describe the directions of the central intensities of the wavevectors and $\gamma_{\mathrm{s,p}}$ are the signal and pump walk-off angles, respectively. The terms

$$\mathcal{N}_{\mathrm{p}} = \frac{\Omega_{\mathrm{p}}}{c} \frac{\mathrm{d}n_{\mathrm{p}}(\Omega_{\mathrm{p}}, \phi)}{\mathrm{d}\phi}\bigg|_{\phi_o} \quad \text{and} \quad \mathcal{N}_{\mathrm{s}} = \frac{\Omega_{\mathrm{s}}}{c} \frac{\mathrm{d}n_{\mathrm{s}}(\Omega_{\mathrm{s}}, \phi)}{\mathrm{d}\phi}\bigg|_{\phi_o + \gamma_{\mathrm{p}}}$$

account for the effects on the refractive indexes of the pump and the signal due to the pump angular spread, which is responsible for a small deviation from the phase-matching angle ϕ_o. The other terms are defined as

$$D = -\frac{\mathrm{d}n_{\mathrm{i}}(\omega_{\mathrm{i}})\omega_{\mathrm{i}}/c}{\mathrm{d}\omega_{\mathrm{i}}}\bigg|_{\Omega_{\mathrm{i}}} + \frac{\mathrm{d}n_{\mathrm{s}}(\omega_{\mathrm{s}}, \phi)\omega_{\mathrm{s}}/c}{\mathrm{d}\omega_{\mathrm{s}}}\bigg|_{\Omega_{\mathrm{s}}} \quad \text{and} \quad \nu = \omega_{\mathrm{s}} - \Omega_{\mathrm{s}} = \Omega_{\mathrm{i}} - \omega_{\mathrm{i}}.$$

Note that $\mathcal{N}_{\mathrm{s}} = \gamma_{\mathrm{s}} = 0$ for type I phase-matching. The first term in the expression for Δk_z accounts for the differential phase velocity between the signal and idler photons in the crystal, which is zero for type I degenerate; the second and third terms are responsible for the pump and signal walk-offs, respectively. (The signal and idler walk-offs are generally equal to zero for type I.) The fourth term accounts for the pump transverse distribution as an angular spread around a principal direction, and the last two terms are associated with the non-collinear

emission of the photons. We note that, in the type I degenerate case, these last two terms cancel out.

The pump beam transverse field distribution is defined via the Fourier transform

$$E_{\mathrm{p}}(\boldsymbol{\rho}) = \frac{1}{2\pi}\int \mathrm{d}^2 q_{\mathrm{p}}\, \widetilde{E}_{\mathrm{p}}(\boldsymbol{q}_{\mathrm{p}})\mathrm{e}^{\mathrm{i}\boldsymbol{q}_{\mathrm{p}}\cdot\boldsymbol{\rho}}. \tag{19}$$

We take this transverse distribution to be Gaussian having a waist of w_{p} at the crystal, and assume that the transverse crystal size is large relative to the pump beam; therefore we can take the cross-section S to be infinite. Moreover, we assume that the pump beam has a narrow angular spectrum (transverse wavevector distribution) and the signal and idler are observed only at points close to their central directions. The central frequencies are $\Omega_{\mathrm{s,i}}$. We also assume that the pump propagates with negligible diffraction inside the crystal, so that $E_{\mathrm{p}}(\boldsymbol{\rho})$ is independent of z. With these approximations, we calculate the valid ranges of w_{p}, L and w_o, which is the width of collection fibre mode as imaged at the crystal. In particular, $L \ll K_{\mathrm{p}} w_{\mathrm{p}}^2/2$ to have negligible diffraction of the pump in the crystal. We can neglect second-order terms in the transverse wavevector component in equations (18) when $w_{o,\mathrm{p}} \gg (K_{\mathrm{s,i}}\gamma_{\mathrm{p,s}})^{-1}$ and, in the non-collinear case, when $w_{o,\mathrm{p}} \gg (K_{\mathrm{s,i}}\theta_{\mathrm{s,i}})^{-1}$.

Using these approximations, we rewrite equation (15) as

$$|\psi\rangle = N\int_{-L}^{0}\mathrm{d}z\int \mathrm{d}^2 q_{\mathrm{s}}\,\mathrm{d}^2 q_{\mathrm{i}}\,\mathrm{d}^2 q_{\mathrm{p}}\,\mathrm{d}\nu\,\widetilde{E}_{\mathrm{p}}(\boldsymbol{q}_{\mathrm{p}})\mathrm{e}^{\mathrm{i}\Delta k_z z}\delta(\Delta k_x)\delta(\Delta k_y)|1_{\boldsymbol{k}_{\mathrm{s}},\omega_{\mathrm{s}}}\rangle|1_{\boldsymbol{k}_{\mathrm{i}},\omega_{\mathrm{i}}}\rangle. \tag{20}$$

To evaluate C_{12} and $S_{1,2}$, we rewrite the state $|\psi\rangle$ in terms of $|1_{\boldsymbol{r}_1,t_1}\rangle|1_{\boldsymbol{r}_2,t_2}\rangle$ by using

$$|1_{\boldsymbol{k}_{\mathrm{s}},\omega_{\mathrm{s}}}\rangle = \frac{1}{(2\pi)^2}\int \mathrm{d}^3 r_1\,\mathrm{d}t_1\,\mathrm{e}^{\mathrm{i}(\boldsymbol{k}_{\mathrm{s}}\cdot\boldsymbol{r}_1-\omega_{\mathrm{s}}t_1)}|1_{\boldsymbol{r}_1,t_1}\rangle \tag{21}$$

and

$$|1_{\boldsymbol{k}_{\mathrm{i}},\omega_{\mathrm{i}}}\rangle = \frac{1}{(2\pi)^2}\int \mathrm{d}^3 r_2\,\mathrm{d}t_2\,\mathrm{e}^{\mathrm{i}(\boldsymbol{k}_{\mathrm{i}}\cdot\boldsymbol{r}_2-\omega_{\mathrm{i}}t_2)}|1_{\boldsymbol{r}_2,t_2}\rangle. \tag{22}$$

Thus the $\Phi(\boldsymbol{k}_{\mathrm{s}},\boldsymbol{k}_{\mathrm{i}},\omega_{\mathrm{i}},\omega_{\mathrm{s}})$ in equation (16) becomes, in the new basis, its Fourier transform $\widetilde{\Phi}(\boldsymbol{r}_1,\boldsymbol{r}_2,t_1,t_2)$, as indicated formally in equation (2) and calculated at the output surface of the crystal ($z_{1,2}=0$). By first performing the Fourier transforms and leaving the z integration for performing last, we obtain

$$\begin{aligned}\widetilde{\Phi}(\boldsymbol{r}_1,\boldsymbol{r}_2,t_1,t_2) = N_1\exp\left[\frac{-\mathrm{i}(K_{\mathrm{i}}\theta_{\mathrm{i}}^2+K_{\mathrm{s}}(\theta_{\mathrm{s}}\theta_{\mathrm{i}}-\gamma_{\mathrm{s}}\gamma_{\mathrm{p}}))\tau}{D}\right]\exp\left[\frac{-(\mathcal{N}_{\mathrm{p}}-\mathcal{N}_{\mathrm{s}})^2\tau^2}{D^2 w_{\mathrm{p}}^2 K_{\mathrm{p}}}\right]\\ \times\exp\left[\frac{2(\mathcal{N}_{\mathrm{p}}-\mathcal{N}_{\mathrm{s}})\tau(y_1+\frac{\theta_{\mathrm{i}}\tau}{D})}{D w_{\mathrm{p}}^2 K_{\mathrm{p}}}\right]\exp\left[-\frac{x_1^2+(y_1+\frac{\theta_{\mathrm{i}}\tau}{D})^2}{w_{\mathrm{p}}^2}\right]\Pi_{DL}(\tau)\\ \times\delta\left(x_1-x_2-\frac{\gamma_{\mathrm{s}}\tau}{D}\right)\delta\left(y_1-y_2+\frac{(\theta_{\mathrm{i}}+\theta_{\mathrm{s}})\tau}{D}\right)\delta(z_1)\delta(z_2),\end{aligned} \tag{23}$$

where $\tau = t_1 - t_2$ and $\Pi_{DL}(\tau) = 1$ for $0 \leqslant \tau \leqslant DL$ and 0 elsewhere. To guarantee that the biphoton state is properly normalized, the factor N_1 is determined from the condition $\int \mathrm{d}^3 r_1\, \mathrm{d}^3 r_2\, \mathrm{d}t_1\, \mathrm{d}t_2\, |\widetilde{\Phi}(\boldsymbol{r}_1, \boldsymbol{r}_2, t_1, t_2)|^2 = 1$, yielding $N_1 = w_\mathrm{p}/4\pi^2\sqrt{DL}$. To calculate the field-based collection efficiency, we assume that the guided mode is a Gaussian field at the crystal output surface, defined by

$$\varphi^*_{10}(x_j, y_j) = \sqrt{\frac{2}{\pi}}\frac{1}{w_o}\exp\left[-\frac{(x_j^2 + y_j^2)}{w_o^2}\right]. \tag{24}$$

The imaging optic is arranged to place the collection beam waist w_o at the crystal. The intensity of the collection modes is normalized by setting $\int [\varphi^*_{10}]^2\, \mathrm{d}x\, \mathrm{d}y = 1$, which yields the coefficient in equation (24). The biphoton field is calculated using equations (1), (3) and (23), and the operator

$$\hat{a}_{\boldsymbol{k}_{\mathrm{s,i}},\omega_{\mathrm{s,i}}} = \frac{1}{(2\pi)^2}\int \mathrm{d}^3 r_{1,2}\, \mathrm{d}t_{1,2}\, \hat{a}_{\boldsymbol{r}_{1,2},t_{1,2}}\, \mathrm{e}^{-\mathrm{i}\boldsymbol{k}_{\mathrm{s,i}}\cdot\boldsymbol{r}_{1,2} + \omega_{\mathrm{s,i}} t_{1,2}} \tag{25}$$

to obtain

$$A_{12}(\boldsymbol{r}_1, \boldsymbol{r}_2, t_1, t_2) \propto N_E^2 \widetilde{\Phi}(\boldsymbol{r}_1, \boldsymbol{r}_2, t_1, t_2). \tag{26}$$

The single-mode field-based collection efficiency is then given by

$$\chi_{12} = \mathcal{F}\frac{4w_o w_\mathrm{p}^2\sqrt{(w_o^2 + w_\mathrm{p}^2)(-\mathcal{N}_\mathrm{p} + \mathcal{N}_\mathrm{s} + K_\mathrm{p}\theta_\mathrm{i})\sqrt{K_\mathrm{p}^2\gamma_\mathrm{s}^2 + (\mathcal{N}_\mathrm{p} - \mathcal{N}_\mathrm{s} + K_\mathrm{p}\theta_\mathrm{s})^2}}}{\sqrt{(w_o^2 + 2w_\mathrm{p}^2)^3 B}}, \tag{27}$$

with

$$\mathcal{F} = \frac{\mathrm{Erf}\left[\dfrac{L\sqrt{B}}{K_\mathrm{p} w_o\sqrt{w_o^2/2 + w_\mathrm{p}^2}}\right]}{\sqrt{\mathrm{Erf}\left[\sqrt{2}L\dfrac{(-\mathcal{N}_\mathrm{p} + \mathcal{N}_\mathrm{s} + K_\mathrm{p}\theta_\mathrm{i})}{K_\mathrm{p}\sqrt{w_o^2 + w_\mathrm{p}^2}}\right]\mathrm{Erf}\left[\sqrt{2}L\dfrac{\sqrt{K_\mathrm{p}^2\gamma_\mathrm{s}^2 + (\mathcal{N}_\mathrm{p} - \mathcal{N}_\mathrm{s} + K_\mathrm{p}\theta_\mathrm{s})^2}}{K_\mathrm{p}\sqrt{w_o^2 + w_\mathrm{p}^2}}\right]}}, \tag{28}$$

and $B = (2\mathcal{N}_\mathrm{p}^2 + 2\mathcal{N}_\mathrm{s}^2 - 2\mathcal{N}_\mathrm{p}(2\mathcal{N}_\mathrm{s} + K_\mathrm{p}(\theta_\mathrm{i} - \theta_\mathrm{s})) + 2K_\mathrm{p}\mathcal{N}_\mathrm{s}(\theta_\mathrm{i} - \theta_\mathrm{s}) + K_\mathrm{p}^2(\gamma_\mathrm{s}^2 + \theta_\mathrm{i}^2 + \theta_\mathrm{s}^2))w_o^2 + K_\mathrm{p}^2(\gamma_\mathrm{s}^2 + (\theta_\mathrm{i} + \theta_\mathrm{s})^2)w_\mathrm{p}^2$. In the thin crystal limit, this reduces to

$$\chi_{12} = \frac{4w_\mathrm{p}^2(w_o^2 + w_\mathrm{p}^2)}{(w_o^2 + 2w_\mathrm{p}^2)^2} \tag{29}$$

as first calculated in [23, 24]. In this approach, the fibres act to project the photon's state onto a specific propagation mode both in amplitude and phase, as indicated in equations (7) and (8). The spatial coherence of the single guided modes in the signal and idler arms should ultimately match the overall spatial coherence of the two-photon states.

4. Calculation of the single-mode intensity-based collection efficiency

To calculate the single-mode intensity-based collection efficiency, we assume that the projectors $\widehat{P}_j$, representing the fibre modes propagated back to the output surface of the crystal, are completely determined by the functions

$$\mathcal{I}_j(\boldsymbol{r}_j) = \mathrm{e}^{-2(x_j^2+y_j^2)/w_j^2}\delta(z_j). \tag{30}$$

(Note that in this approach, the intensity projection operator has a maximum of 1 because of its probabilistic nature.) Assuming that the conditions detailed following equation (19) are valid and $w_\mathrm{s} = w_\mathrm{i} = w_o$, we calculate the single-mode intensity-based collection efficiency

$$\eta_{12} = \mathcal{F}\frac{w_o\sqrt{(w_o^2+w_\mathrm{p}^2)(-\mathcal{N}_\mathrm{p}+\mathcal{N}_\mathrm{s}+K_\mathrm{p}\theta_\mathrm{i})\sqrt{K_\mathrm{p}^2\gamma_\mathrm{s}^2+(\mathcal{N}_\mathrm{p}-\mathcal{N}_\mathrm{s}+K_\mathrm{p}\theta_\mathrm{s})^2}}}{\sqrt{(w_o^2+2w_\mathrm{p}^2)B}}. \tag{31}$$

In the thin crystal limit, η_{12} becomes

$$\eta_{12} = \frac{w_o^2+w_\mathrm{p}^2}{(w_o^2+2w_\mathrm{p}^2)}. \tag{32}$$

Note that there are several approximations other than $L \to 0$ that lead to equation (32). For example, the assumptions following equation (19) preclude the case of an arbitrarily small pump waist at the crystal. The collection mode waist is also restricted to modes that can be created by finite lenses that image fibres at a finite distance from the crystal.

In the intensity-based approach presented in this section, the collection mode can be considered as spatially filtering the multi-mode input light. Thus it is likely better suited for modelling the multi-mode fibre collection. As the next section demonstrates, the predictions made by this model yield different results than the field-based model. The intensity-based model predicts that, for a fixed pump waist, the maximum collection efficiency is obtained when the fibre-defined collection mode (at the crystal) is large, i.e. all the pumped crystal volume is in a region of unit collection efficiency of the fibre/spatial filter system. With the field-based approach, the optics set-up of figure 1 can be envisioned in an unfolded geometric arrangement [28], where one of the fibres acts as a single-mode source propagating back through a spatial filter (in this case, the pumped crystal volume) to the other fibre. The maximum collection is achieved with a large pump waist, with respect to the collection beam waist at the crystal. If the pump waist is smaller than the fibre-defined collection beam waist, the collection efficiency is decreased. It is probable that the field-based approach gives the best answers for a single-mode fibre. However, moving to multi-mode fibres, the result should approach the intensity-based model, i.e. corresponding to a statistical optics physical description.

5. Discussion of results

The most immediately obvious result in this paper is that in the thin crystal limit, η_{12} and χ_{12} provide totally different predictions. Figure 2 shows the field- and intensity-based collection

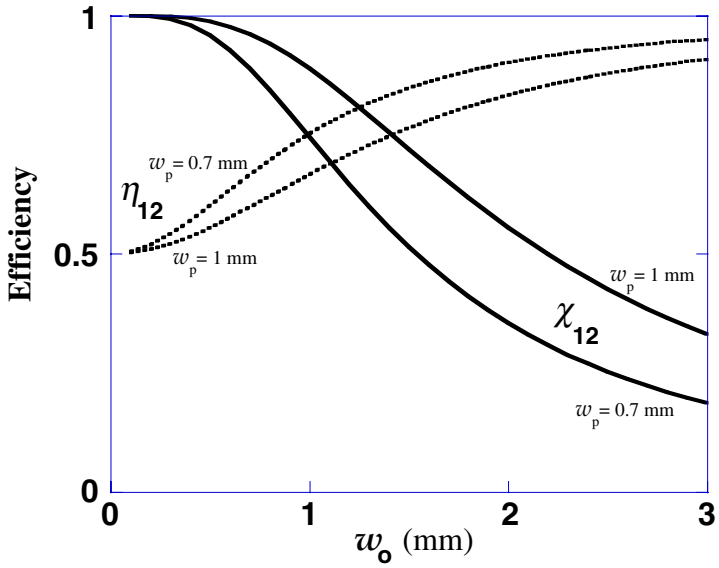

Figure 2. Field-based (——) and intensity-based collection efficiencies (· · · · · ·) in the thin crystal limit versus w_o for fixed values of w_p.

efficiencies compared with the collection mode waists for fixed values of pump waist. When the collection waist is much greater than the pump waist, η_{12} asymptotically tends to 1, whereas χ_{12} tends to 0; in the opposite condition ($w_p \gg w_o$), $\eta_{12} \to \frac{1}{2}$ and $\chi_{12} \to 1$. However, the thin crystal approximation is far from valid unless the crystal is shorter than 0.1 mm for these collection beam diameters. In practical cases, crystal lengths range from 0.5 to 20 mm. This is one of the prime motivations for this work.

To illustrate a practical lab set-up, we consider a BBO crystal with type I and II phase-matchings pumped at 458 nm and look at down-conversion at the degenerate wavelength (916 nm). For both types I and II, we describe the collinear and non-collinear cases with $\theta_s = \theta_i \cong 1.5^\circ$. To make valid predictions, we must ensure that the combination of L and w_p satisfy the assumptions made in deriving the expression. Figure 3 shows a graph of valid parameter combinations, generally putting a lower limit on the size of the pump waist.

Figure 4 plots both η_{12} and χ_{12} versus w_o for fixed $w_p = 0.1$ mm and crystal lengths of $L = 1$ and 10 mm, with their limit values referring to the thin crystal approximation. Cases of collinear and non-collinear configurations for both type I (figure 4, upper panel) and type II (figure 4, lower panel) phase-matchings are plotted. Again, note the different behaviours of η_{12} and χ_{12}. When a crystal longer than 0.1 mm is used, both η_{12} and χ_{12} can be significantly decreased if the pump and collection waists are not properly matched. The way to match the waist for the optimum collection efficiency is different for η_{12} and χ_{12}. In particular, η_{12} can be optimized for a long crystal by increasing the collection waist at the crystal. The opposite holds for χ_{12}. Moreover, for η_{12} in the case of type I phase-matching (figure 4, upper panel), we observe that the collinear configuration always guarantees a better coupling, whereas this is not the case with type II. This can be observed for η_{12} evaluated at $L = 10$ mm in figure 4 (lower panel): for $w_o < 0.5$ mm, the non-collinear configuration appears to be clearly more efficient compared with the collinear one. We can justify this behaviour, because in type II collinear phase-matching, the walk-off angle of the signal is less compared with that in the non-collinear configuration.

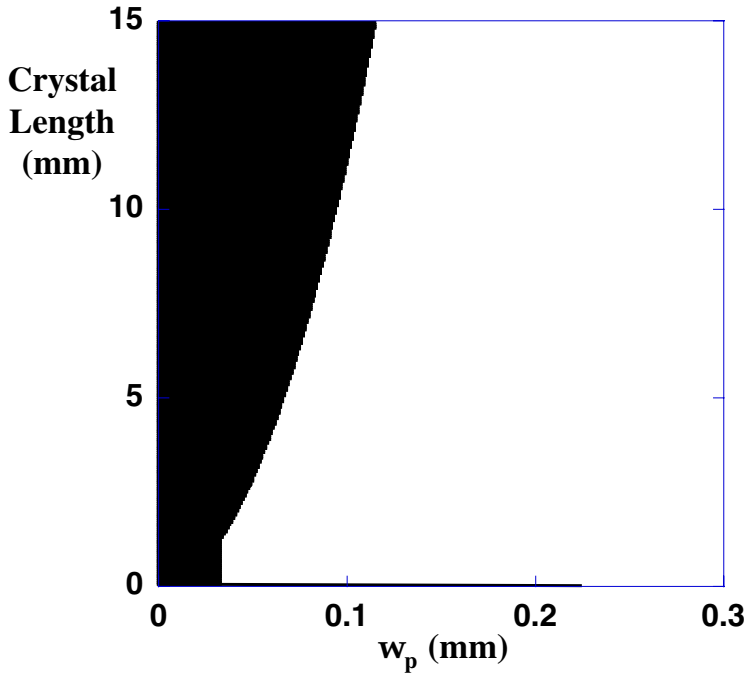

Figure 3. A plot of the range of values for L and w_{p} to guarantee the validity of the final formula (white region). Calculations are within the conditions of $w_o \geqslant w_{\mathrm{p}}$ (a trivial, convenient experimental choice) and non-collinear phase-matching for the angles and frequencies given in section 5.

Figure 5 shows effects of the crystal length on η_{12} and χ_{12} with $w_{\mathrm{p}} = w_o = 0.2$ and 0.4 mm. We observe that, apart from their different values, η_{12} and χ_{12} present completely analogous dependences on the length of the crystal: all the chosen configurations, namely types I and II, collinear and non-collinear, converge to the thin crystal curve for very short lengths, whereas for long crystals, they reach different lower asymptotic values depending on the associated waist configurations. In fact, for $L \to \infty$, the factor $\mathcal{F}$ in equation (28) approaches 1; thus the long crystal asymptotic values can be obtained directly from equations (31) and (27).

In general, the coupling efficiencies are higher in type I compared with type II, although for long crystals, there is a noticeable behaviour difference between types I and II. For type I, collinear geometry yields the best coupling efficiencies, whereas for type II, non-collinear geometry is best. However, the discrepancy between type II collinear and non-collinear configurations is less evident for crystals of intermediate length. It is noteworthy to observe that the dependence on the crystal length is actually re-scalable by scaling the pump and collection waists.

Figure 6 plots χ_{12} and η_{12} versus w_o and w_{p} for two different lengths of the crystal. For χ_{12}, we have an optimum match between w_o and w_{p} (maximizing collection efficiency) with type II phase-matching. This is clear from figure 6(b), where the crystal length is 10 mm. For η_{12}, we did not find a similar behaviour even for a wider range of w_{p} and w_o.

Because of other effects that can lower the efficiency in practice (such as crystal and optical losses, detector inefficiencies and so on [29]), it is important to make an experimental test of the theory that is not sensitive to these extraneous types of losses. With this view, it is best

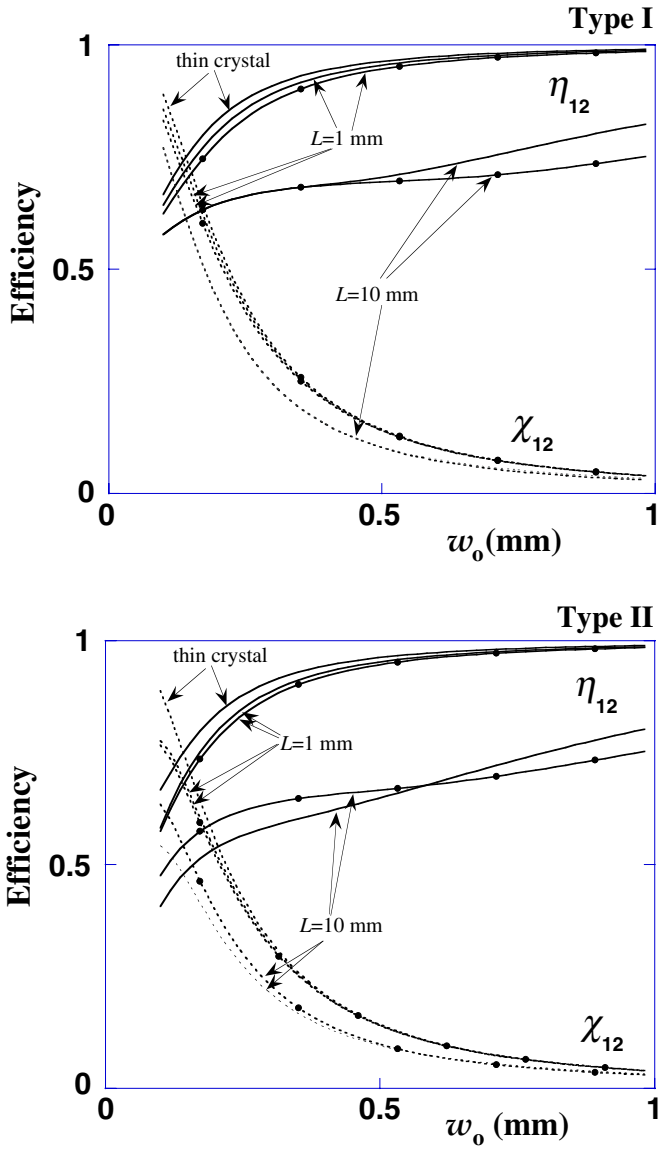

Figure 4. Plot of η_{12} (——) and χ_{12} (- - - -) versus w_o for fixed $w_p = 100\,\mu$m and $L = 1$ and 10 mm. We simulated the case of type I (upper panel) for collinear and non-collinear conditions (with dots) with $\gamma_p = 3.5^\circ$ and $\mathcal{N}_p = -1.4\,\mu\text{m}^{-1}$. We simulated the case of type II (lower panel) for collinear and non-collinear conditions (with dots) with $\gamma_p = 4.28^\circ$, $\gamma_s = 4.07^\circ$, $\mathcal{N}_p = -1.67\,\mu\text{m}^{-1}$ and $\mathcal{N}_s = -0.77\,\mu\text{m}^{-1}$.

to choose a configuration where the two models have opposite dependences on adjustable experimental parameters. For example, one could measure the collection efficiency for fixed crystal lengths, while varying either the pump waist or the collection waist, such as in the central value range of figure 4. A type II configuration could be useful to outline further the differences, as demonstrated in figure 6, where an optimum pump-collection waist is predicted only in one case.

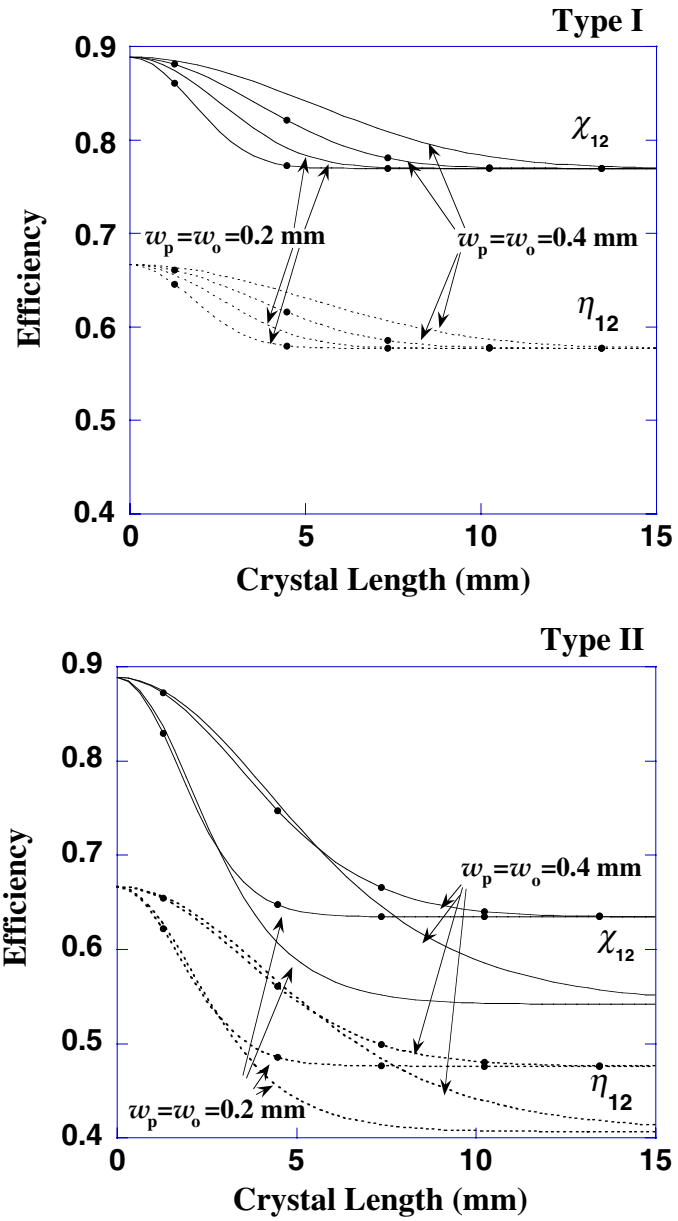

Figure 5. Plots of η_{12} (- - - -) and χ_{12} (——) versus L for fixed $w_p = w_o = 0.2$ and 0.4 mm. We simulated the cases of type I (upper panel) and type II (lower panel). Both non-collinear (as indicated by the curves with dots) and collinear (curves without dots) PDC output configurations were calculated with all other parameters the same as in figure 4.

6. Conclusions

We have presented an analytical model to quantify the collection efficiency in terms of adjustable experimental parameters with the goal of optimizing single-mode collection from two-photon sources. An alternative scheme is also presented that may have more validity for multi-mode collection arrangements. Our calculation was performed using generally accepted

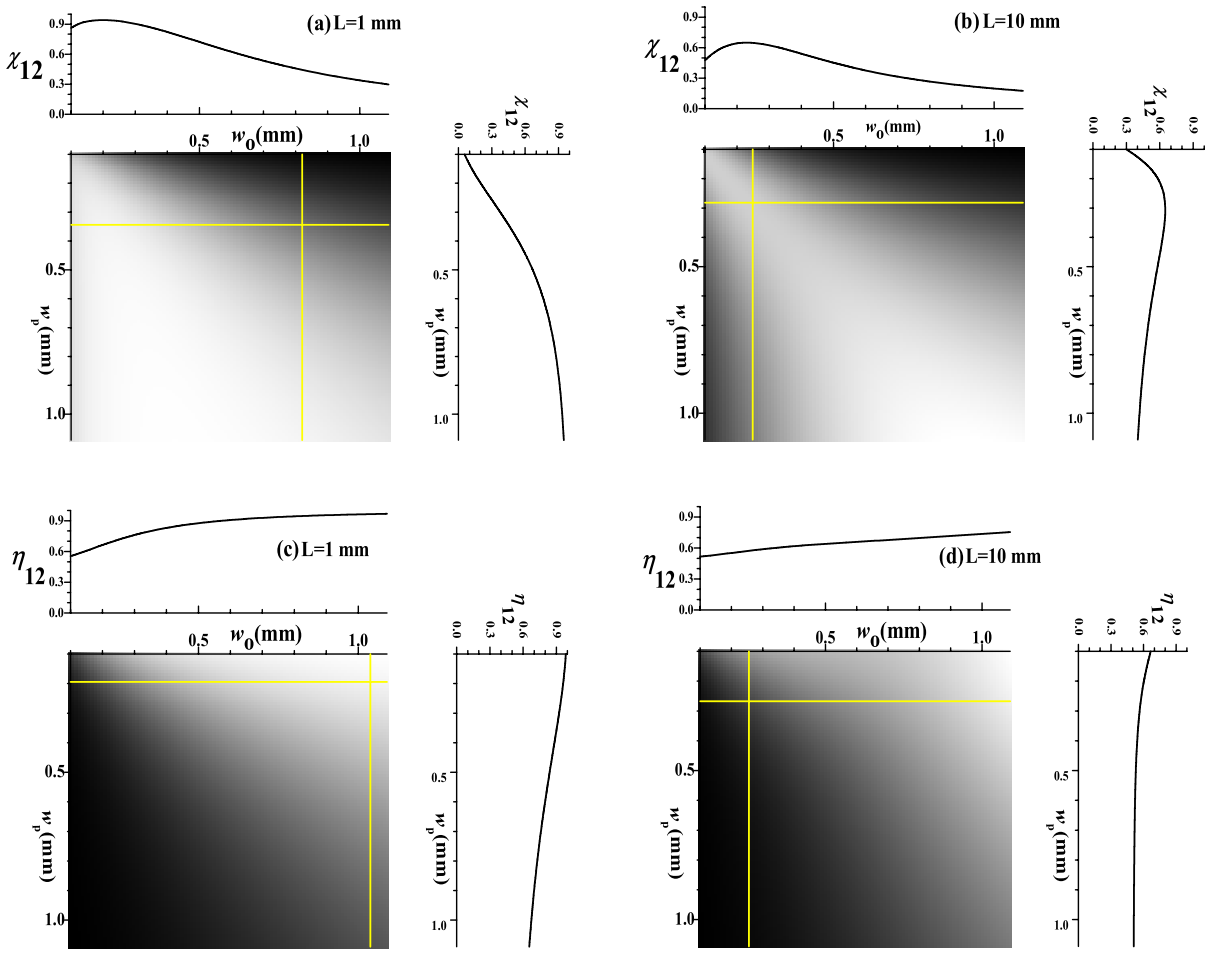

Figure 6. Density plots of χ_{12} (a, b) and η_{12} (c, d) versus w_o, w_p for $L = 1$ mm (a, c) and 10 mm (b, d), respectively for type II non-collinear phase-matching. The lighter area corresponds to higher efficiency.

approximations, such as relying mainly on a finite transverse distribution of the fields involved and neglecting second-order terms in the components of the transverse-wave vector. These calculations cover a wide range of experimental configurations and yield two formulae to quantify the collection efficiencies. We have pointed out the experimental conditions that could be used to differentiate between the two models.

Acknowledgments

This work was supported in part by DARPA/QUIST, ARDA and ARO and partially by Elsag SpA/Qcrypt.

Appendix

Here we present the calculations to obtain Δk_x, Δk_y and Δk_z in equations (18). As shown in figure A.1, we consider a uniaxial negative crystal with a pump beam propagating as an

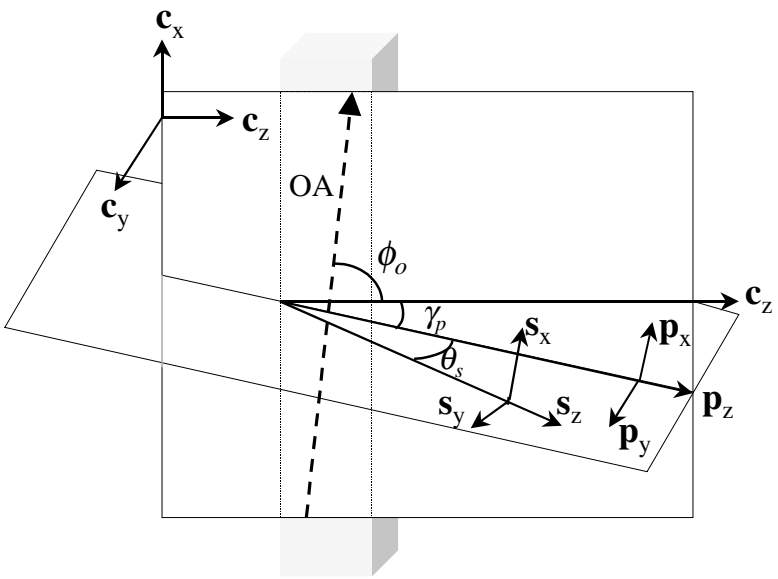

Figure A.1. Non-collinear type I phase-matching in uniaxial negative crystals; see the text for details.

extraordinary ray. Hereinafter, we adopt the crystal directions ($\boldsymbol{c}_{x,y,z}$) as a co-ordinate system for subsequent calculations with the pump beam oriented along $\boldsymbol{c}_z$. Because of walk-off, the direction of propagation of the pump does not coincide with $\boldsymbol{c}_z$, but is deflected by an angle γ_p. Therefore its direction of propagation is $\boldsymbol{p}_z = (\sin\gamma_\mathrm{p}, 0, \cos\gamma_\mathrm{p})^\mathrm{T}$, and the associated transverse directions are $\boldsymbol{p}_x = (\cos\gamma_\mathrm{p}, 0, -\sin\gamma_\mathrm{p})^\mathrm{T}$ and $\boldsymbol{p}_y = \boldsymbol{c}_y$ (T stands for transpose). This is simply a rotation around the direction $\boldsymbol{c}_y$ by an angle γ_p.

We first analyse the case of type I non-collinear PDC, where both signal and idler are ordinary rays, and we restrict the signal and idler directions to the plane perpendicular to the principal plane of the crystal (the plane defined by the pump wave vector and the optic axis of the crystal). Although these geometry restrictions are used to simplify the calculations for illustrative purposes, they do not affect the overall conclusions. The calculations can be extended straightforwardly to a general geometry configuration and to type II phase-matching.

We assume also that the signal photons are emitted at an angle θ_s with respect to the pump direction as depicted in figure A.1. By performing a rotation of the pump directions around $\boldsymbol{p}_x$ by an angle θ_s, we deduce the direction of propagation of the signal as $\boldsymbol{s}_z = (\cos\theta_\mathrm{s}\sin\gamma_\mathrm{p},\ \sin\theta_\mathrm{s},\ \cos\theta_\mathrm{s}\cos\gamma_\mathrm{p})^\mathrm{T}$ and the associated transverse directions as $\boldsymbol{s}_x = \boldsymbol{p}_x$ and $\boldsymbol{s}_y = (-\sin\theta_\mathrm{s}\sin\gamma_\mathrm{p}, \cos\theta_\mathrm{s}, -\sin\theta_\mathrm{s}\cos\gamma_\mathrm{p})$. The same holds for the idler ($\boldsymbol{i}_z$ is the direction of propagation, $\boldsymbol{i}_x$ and $\boldsymbol{i}_y$ are the transverse directions) by simply replacing θ_s with θ_i.

For type II non-collinear parametric phase-matching, the idler is an ordinary ray (with the same considerations above), whereas the signal is an extraordinary ray. This means that the projection of the signal wavevector along $\boldsymbol{c}_z$ is additionally rotated by an angle γ_s because of the crystal birefringence. In this case again, by performing this extra rotation, the direction of propagation of the signal is evaluated as

$$\begin{aligned}\boldsymbol{s}_z = (&\cos\theta_\mathrm{s}\cos\gamma_\mathrm{p}\sin\gamma_\mathrm{s} + \cos\theta_\mathrm{s}\sin\gamma_\mathrm{p}\cos\gamma_\mathrm{s},\ \sin\theta_\mathrm{s},\\ &\cos\theta_\mathrm{s}\cos\gamma_\mathrm{p}\cos\gamma_\mathrm{s} - \cos\theta_\mathrm{s}\sin\gamma_\mathrm{p}\sin\gamma_\mathrm{s})^\mathrm{T}\end{aligned} \tag{A.1}$$

with the associated transverse directions

$$\begin{aligned}\boldsymbol{s_x} &= (\cos\gamma_\mathrm{p}\cos\gamma_\mathrm{s} - \sin\gamma_\mathrm{p}\sin\gamma_\mathrm{s}, 0, -\cos\gamma_\mathrm{p}\sin\gamma_\mathrm{s} - \sin\gamma_\mathrm{p}\cos\gamma_\mathrm{s})^\mathrm{T},\\ \boldsymbol{s_y} &= (-\sin\theta_\mathrm{s}\cos\gamma_\mathrm{p}\sin\gamma_\mathrm{s} - \sin\theta_\mathrm{s}\sin\gamma_\mathrm{p}\cos\gamma_\mathrm{s}, \cos\theta_\mathrm{s},\\ &\quad -\sin\theta_\mathrm{s}\cos\gamma_\mathrm{p}\cos\gamma_\mathrm{s} + \sin\theta_\mathrm{s}\sin\gamma_\mathrm{p}\sin\gamma_\mathrm{s})^\mathrm{T}.\end{aligned}$$

Here we describe the approximations leading to the final equations (18). We apply to equation (17) the paraxial approximation along the longitudinal directions of the pump, signal and idler fields. We assume that the signal and idler waves in these directions are narrow band and reached a peak around the frequencies Ω_s and Ω_i respectively and the pump beam is in a single-frequency mode (Ω_p) (this, of course, is wrong for a pulsed pump beam).

As other authors have done, we account for dependence of the extraordinary wave's index of refraction on the angle between the optic axis and the component of the direction of propagation of the wave in the principal plane of the crystal (called phase-matching angle). This means that, because the angular spread of the pump beam gives a phase-matching angle not uniquely determined, we have to evaluate this dependence by expanding the indexes of refraction around the central phase-matching angle, specifically ϕ_o and $\phi_o + \gamma_\mathrm{p}$ for the pump and the signal (when we deal with type II), respectively. With this assumption, equation (17) becomes the following for each field:

$$\begin{aligned}\boldsymbol{k}_\mathrm{p}\cdot\boldsymbol{p}_z &= K_\mathrm{p}\left(1 - \frac{\boldsymbol{q}_\mathrm{p}^2}{2K_\mathrm{p}^2}\right) + (\phi-\phi_o)\mathcal{N}_\mathrm{p} + \cdots,\\ \boldsymbol{k}_\mathrm{s}\cdot\boldsymbol{s}_z &= K_\mathrm{s}\left(1 - \frac{\boldsymbol{q}_\mathrm{s}^2}{2K_\mathrm{s}^2}\right) + \left.\frac{\mathrm{d}n_\mathrm{s}(\omega_\mathrm{s},\phi)\omega_\mathrm{s}/c}{\mathrm{d}\omega_\mathrm{s}}\right|_{\Omega_\mathrm{s}}(\omega_\mathrm{s}-\Omega_\mathrm{s})\\ &\quad + \frac{1}{2}\left.\frac{\mathrm{d}^2 n_\mathrm{s}(\omega_\mathrm{s},\phi)\omega_\mathrm{s}/c}{\mathrm{d}\omega_\mathrm{s}^2}\right|_{\Omega_\mathrm{s}}(\omega_\mathrm{s}-\Omega_\mathrm{s})^2 + (\phi-\phi_o-\gamma_\mathrm{p})\mathcal{N}_\mathrm{s} + \cdots, \qquad \text{(A.2)}\\ \boldsymbol{k}_\mathrm{i}\cdot\boldsymbol{i}_z &= K_\mathrm{i}\left(1 - \frac{\boldsymbol{q}_\mathrm{i}^2}{2K_\mathrm{i}^2}\right) + \left.\frac{\mathrm{d}n_\mathrm{i}(\omega_\mathrm{i})\omega_\mathrm{i}/c}{\mathrm{d}\omega_\mathrm{i}}\right|_{\Omega_\mathrm{i}}(\omega_\mathrm{i}-\Omega_\mathrm{i})\\ &\quad + \frac{1}{2}\left.\frac{\mathrm{d}^2 n_\mathrm{i}(\omega_\mathrm{i})\omega_\mathrm{i}/c}{\mathrm{d}\omega_\mathrm{i}^2}\right|_{\Omega_\mathrm{i}}(\omega_\mathrm{i}-\Omega_\mathrm{i})^2 + \cdots,\end{aligned}$$

where

$$\mathcal{N}_\mathrm{p} = \left.\frac{\Omega_\mathrm{p}}{c}\frac{\mathrm{d}n_\mathrm{p}(\Omega_\mathrm{p},\phi)}{\mathrm{d}\phi}\right|_{\phi_o} \quad\text{and}\quad \mathcal{N}_\mathrm{s} = \left.\frac{\Omega_\mathrm{s}}{c}\frac{\mathrm{d}n_\mathrm{s}(\Omega_\mathrm{s},\phi)}{\mathrm{d}\phi}\right|_{\phi_o+\gamma_\mathrm{p}}.$$

We limited our calculation to the first perturbative order for all the variables involved, i.e. for the frequency, the transverse wavevector components and the angles. We observe that we can go back to type I phase-matching by setting $\mathcal{N}_\mathrm{s} = \gamma_\mathrm{s} = 0$. Furthermore, we can approximate $\phi - \phi_o - \gamma_\mathrm{p} \simeq \phi - \phi_o \simeq \boldsymbol{q}_\mathrm{p}\cdot\boldsymbol{p_y}/K_\mathrm{p}$.

Finally, we use the sine and cosine terms in the $\boldsymbol{p}$, $\boldsymbol{s}$ and $\boldsymbol{i}$ component directions written in the crystal reference system to their first perturbative order, because of the assumed small emission and birefringence angles (about a few degrees). We then calculate $\Delta k_{x,y,z} = (\boldsymbol{k}_\mathrm{p} - \boldsymbol{k}_\mathrm{s} - \boldsymbol{k}_\mathrm{i}) \cdot \boldsymbol{c}_{x,y,z}$, obtaining equations (18) directly.

References

[1] Bennett C and Brassard G 1984 *Proc. IEEE Int. Conf. on Computers, Systems and Signal Processing, Bangalore* p 175
[2] Bennett C and Brassard G 1985 *IBM Technical Disclosure Bull.* **28** 3153
[3] Bennett C and Brassard G 1989 *SIGACT NEWS* **20** 78
[4] Bennett C H, Bessette F, Brassard G, Salvail L and Smolin J 1991 *Lecture Notes in Computer Science* **473** 253
[5] Ekert A 1991 *Phys. Rev. Lett.* **67** 661
[6] Bennett C 1992 *Phys. Rev. Lett.* **68** 3121
[7] Bennett C H, Brassard G and Mermin N D 1992 *Phys. Rev. Lett.* **68** 557
[8] Ekert A K, Rarity J G, Tapster P R and Palma G M 1992 *Phys. Rev. Lett.* **69** 1293
[9] Tittel W, Brendel J, Zbinden H and Gisin N 2000 *Phys. Rev. Lett.* **84** 4737
[10] Knill E, Laflamme R and Milburn G J 2001 *Nature* **409** 46
[11] Brassard G, Lutkenhaus N, Mor T and Sanders B C 2000 *Phys. Rev. Lett.* **85** 1330
[12] Jacobs B C and Franson J D 1996 *Opt. Lett.* **21** 1854
[13] Kim J, Benson O, Kan H and Yamamoto Y 1999 *Nature* **397** 500
[14] Kurtsiefer C, Mayer S, Zarda P and Weinfurter H 2000 *Phys. Rev. Lett.* **85** 290
[15] Buttler W T, Hughes R J, Lamoreaux S K, Morgan J L, Nordholt J E and Peterson C G 2000 *Phys. Rev. Lett.* **84** 5652
[16] Yaun Z, Kardynal B, Stevenson R, Shields A, Lobo C, Cooper K, Beattie N, Ritchie D and Pepper M 2001 *Science* **10.1126** 1066790
[17] Pittman T B, Jacobs B C and Franson J D 2002 *Phys. Rev.* A **66** 042303
[18] Beveratos A, Bruori R, Gacoin T, Villing A, Poizat J-P and Grangier P 2002 *Phys. Rev. Lett.* **89** 187901
[19] Migdall A, Branning D and Castelletto S 2002 *Phys. Rev.* A **66** 053805
[20] Migdall A L, Castelletto S, Degiovanni I P and Rastello M L 2002 *Appl. Opt.* **41** 2914
[21] Monken C H, Ribeiro P H S and Padua S 1998 *Phys. Rev.* A **57** R2267
[22] Kurtsiefer C, Oberparleiter M and Weinfurter H 2001 *Phys. Rev.* A **6402** 023802
[23] Bovino F A, Varisco P, Colla A M, Castagnoli G, Di Giuseppe G and Sergienko A V 2003 *Opt. Commun.* **227** 343
[24] Castelletto S, Degiovanni I P, Ware M and Migdall A L 2003 *Preprint* quant-ph/0311099; *SPIE Proc. 5161, San Diego* vol 48
[25] Aichele T, Lvovsky A I and Schiller S 2002 *Eur. Phys. J.* D **18** 237
[26] Rubin M H 1996 *Phys. Rev.* A **54** 5349
[27] Ghatak A and Thyagarajan K 1998 *Introduction to Fiber Optics* (Cambridge: Cambridge University Press)
[28] Klyskho D N 1988 *Phys. Lett.* A **132** 299
[29] Castelletto S, Degiovanni I P and Rastello M L 2003 *Phys. Rev.* A **67** 022305